

# Capturing an Electron in the Virtual State

Alok Nath Singh,<sup>1,2</sup> Bibek Bhandari,<sup>2</sup> Rafael Sánchez,<sup>3,4,5</sup> and  
Andrew N. Jordan<sup>2,1,6</sup>

<sup>1</sup>*Department of Physics and Astronomy, University of Rochester, Rochester, NY 14627, USA*

<sup>2</sup>*Institute for Quantum Studies, Chapman University, Orange, CA 92866, USA*

<sup>3</sup>*Departamento de Física Teórica de la Materia Condensada, Universidad Autónoma de Madrid, 28049 Madrid, Spain*

<sup>4</sup>*Condensed Matter Physics Center (IFIMAC), Universidad Autónoma de Madrid, 28049 Madrid, Spain*

<sup>5</sup>*Instituto Nicolás Cabrera (INC), Universidad Autónoma de Madrid, 28049 Madrid, Spain*

<sup>6</sup>*The Kennedy Chair in Physics, Chapman University, Orange, CA 92866, USA*

We address a foundational question in quantum mechanics: can a particle be directly found in a classically forbidden virtual state? We instantiate this conceptual question by investigating the traversal of electrons through a tunnel barrier, which we define in a triple quantum dot (TQD) system where the occupation of the central dot is energetically avoided. The motivation behind this setup is to answer whether the central dot is occupied or not during a virtual transition when it is being explicitly monitored. We investigate this problem in two different limits of continuous measurements: the stochastic quantum diffusion and the quantum jump. We find that, even though individual trajectories differ considerably across these limits, measuring leads to a higher occupation in the central dot on average. Our results demonstrate that the act of observation fundamentally reshapes tunneling dynamics, resolving the seeming paradox of detecting a particle in a classically forbidden region: weak measurements partially localize the particle, while strong measurements enforce a discontinuous either/or detection or no detection outcome.

**Introduction**—Quantum tunneling is both a paradigmatic manifestation of the particle/wave aspect of quantum physics, and a deeply puzzling effect from a foundations of physics perspective. Much debate continues about simple questions, such as “How long does a particle remain in the classically forbidden region?” [1–8]. It is well known that measurements of quantum properties yield results that are classically well defined - a particle will be found in a particular position if that is indeed what is being measured. In this Letter, we examine the question of measurements on tunneling particles. If we interrogate *where* a tunneling particle is found as it passes from one side to another of a classically forbidden region, a dichotomy arises: On one hand, if we assume a continuous trajectory - that to pass from point A to point C, the particle must go through point B (having a higher energy than A and C), then a measurement of the particle’s position at point B must reveal itself. In that case, the particle must have sufficient energy to be allowed at the position. Since the particle was assumed to not have a sufficient amount of energy, where did it come from? On the other hand, an opposing possibility is that by the act of looking at position B we simply prevent the tunneling from happening in the first place - the measurement spoils the effect.

In the results presented in this Letter, we will show that depending on *how* the measurement is done, both situations can be manifested. We consider tuning the strength of the measurement from arbitrarily weak to projective. We consider both diffusive and jumpy continuous measurements and discuss how we can infer the behavior of the tunneling particle from the continuous measurement results. To simplify the conceptual presentation above, we consider a line of three tunnel coupled quantum dots where the central dot is energetically higher than the other dots, as sketched in Fig. 1. In such a situation, a tunnel current induced by an electrical bias

across the chain is only possible if an electron transits through the virtual state in the central dot –which plays the role of the classically forbidden potential barrier. The position measurement is realistically made via the charge of the electron. By capacitively coupling the central dot to a nearby electrical conductor that is also electrically biased, we can make real time measurements of the occupation of the central dot in a way whose measurement strength can be tuned from no measurement at all, to a rapid projective measurement of the dot’s occupation. The electrical conductor can function in the diffusive quantum limit when operating in the weakly responding regime, or the quantum jump limit when operating in the tunneling regime and counting transmitted electrons that are only permitted to transport when the central dot is empty. While the basic physics here can be realized in many different analogous physical set-ups, this quantum dot realization is both experimentally realistic and conceptually clear and satisfying.

Related works have explored the lifetime and applications of “virtual states” in quantum dot-based setups. In

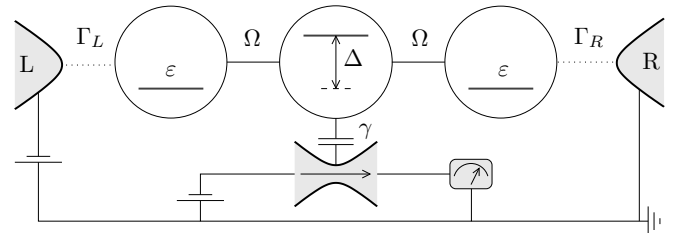


FIG. 1. Scheme of the triple quantum dot coupled to two terminals ( $l = L, R$ ) via tunneling rates  $\Gamma_l$ . The energies of the singly-occupied quantum dots are represented: the central dot is split by  $\Delta$  with respect to the other two, at  $\varepsilon$ . The nearest neighbor hopping is  $\Omega$ . The charge of the central dot is monitored by a coupled QPC measuring with a rate  $\gamma$ .

Refs. [9, 10], the authors examined the lifetime of a virtual state through weak measurements and post-selection based on a classically forbidden cotunneling process in a single quantum dot [11–13]. Studies have also been conducted on double [14] and triple [15] quantum dot setups to investigate virtual states in the context of quantum transport properties. Additionally, virtual states were employed in triple quantum dot (TQD) based setups to demonstrate direct coupling between the outer quantum dots [16–19], showing promise for application in quantum computing. Therefore, while the lifetime of virtual states and their implications for quantum transport and computation have been extensively studied, the consequences of detecting or not detecting a particle in a virtual state remain unexplored. By studying the trajectory of occupation of the monitored virtual state, this paper explores the informational aspects of the existence of the virtual state. We find that in both the diffusive and the jump quantum measurement limit, the measurement back-action results into the central dot being occupied with a much higher probability on average, compared with when there is no measurement. For high measurement strengths, the occupation saturates to a high constant value, while the current through the TQD approaches zero, demonstrating quantum Zeno effect. Our findings indicate that an electron does indeed traverse through the central dot, while going from the left dot to the right dot.

*Model*—We consider a TQD system attached to two electronic reservoirs as shown in Fig. 1. The central dot is continuously monitored by detecting the current through a capacitively-coupled quantum point contact (QPC) [20, 21]. The Hamiltonian for the TQD system is given by

$$\hat{H}_{\text{TQD}} = \sum_i \varepsilon_i \hat{c}_i^\dagger \hat{c}_i - \sum_{i \neq j} \left( \Omega_{ij} \hat{c}_i^\dagger \hat{c}_j + \text{H.c.} \right), \quad (1)$$

where  $\hat{c}_i$  ( $\hat{c}_i^\dagger$ ) are the annihilation (creation) operators for an electron in the quantum dot,  $i = \{L, C, R\}$  with energy  $\varepsilon_i$ .  $\hat{n}_i = \hat{c}_i^\dagger \hat{c}_i$  is the number operator for the quantum dot  $i$  and  $\Omega_{ij}$  gives the tunnel coupling strength between quantum dots  $i$  and  $j$ . We consider symmetric nearest neighbor coupling such that,  $\Omega_{LC} = \Omega_{RC} = \Omega$  whereas  $\Omega_{LR} = 0$ . Additionally, we assume strong onsite and inter-dot Coulomb interaction, much larger than any other energy scale, resulting into a spinless interaction-free Hamiltonian of Eq. (1). The reservoir Hamiltonian can be expressed as,  $\hat{H}_{\text{res}} = \sum_{l=L,R} \sum_k \varepsilon_{k,l} \hat{d}_{k,l}^\dagger \hat{d}_{k,l}$ , where  $\hat{d}_{k,l}$  ( $\hat{d}_{k,l}^\dagger$ ) are the annihilation (creation) operators for an electron with energy  $\varepsilon_{k,l}$  in bath  $l = L, R$ . The TQD system-reservoir coupling is given by,  $\hat{H}_{\text{tun}} = \sum_{l,k} \gamma_l \hat{d}_{k,l}^\dagger \hat{c}_l + \text{h.c.}$ , where  $\gamma_l$  gives the system-reservoir coupling strength.

We consider a configuration where  $\varepsilon_L = \varepsilon_R = \varepsilon$  and  $\varepsilon_C = \varepsilon + \Delta$ , allowing electrons to resonantly transfer from L to R [22]. When  $\Delta \gg \Omega$ , the central dot does not hybridize with the other two, thereby avoiding its occupation. However, direct tunneling between the outer dots remains possible through virtual transitions involving the central dot [16–19]. Thus, the TQD serves as a discrete analog of a tunnel barrier,

with the detuning of the central dot setting the barrier height. A perturbative expansion yields the effective coupling for virtual tunneling as  $\Omega_{\text{eff}} = \Omega^2/\Delta$  [23].

*Diffusive quantum measurement*—We first look at the situation where we make a weak continuous measurement of the occupation of C. Inside the QPC, transmittance of the saddle point constriction depends on whether an electron in C is present (with transmittance  $T_1$ ) or not (with transmittance  $T_0$ ). In the diffusive quantum measurement limit, transmittance is not affected significantly by the occupation, i.e.,  $|T_1 - T_0| \ll (T_1 + T_0)/2$  [24].

Assuming that the coupling to the reservoir is weak, we use the stochastic master equation, in Itô form [24], to evaluate the TQD state evolution,

$$\frac{d\hat{\rho}}{dt} = -\frac{i}{\hbar} [\hat{H}_{\text{TQD}}, \hat{\rho}] + \sum_l (\mathcal{L}_{\Gamma, l+} \hat{\rho} + \mathcal{L}_{\Gamma, l-} \hat{\rho}) + \mathcal{L}_\gamma \hat{\rho}, \quad (2)$$

where  $\mathcal{L}_\lambda = \hat{L}_\lambda \hat{\rho} \hat{L}_\lambda^\dagger - \frac{1}{2} (\hat{L}_\lambda^\dagger \hat{L}_\lambda \hat{\rho} + \hat{\rho} \hat{L}_\lambda^\dagger \hat{L}_\lambda)$  are the usual Lindblad superoperators corresponding to the reservoirs, with the jump operators related to tunneling in,  $\hat{L}_{l+} = \sqrt{\Gamma_{l+}} |l\rangle \langle 0|$ , or tunneling out,  $\hat{L}_{l-} = \sqrt{\Gamma_{l-}} \langle 0| \langle l|$ , of quantum dot  $l = L, R$ . The tunneling rates are given by  $\Gamma_{l+} = \Gamma_l f(\varepsilon_l - \mu_l)$  and  $\Gamma_{l-} = \Gamma_l [1 - f(\varepsilon_l - \mu_l)]$ , where  $f(E) = [1 + \exp\{(E/k_B T)\}]^{-1}$  is the Fermi function and  $\mu_l$  is the electrochemical potential of reservoir  $l$ .  $\Gamma_l = 2\pi \hbar^{-1} |\gamma_l|^2 \nu_l$ , with  $\nu_l$  being the density of states in lead  $l$ , is the tunneling rate between the dot  $l$  and reservoir  $l$ . The Lindblad superoperator corresponding to the measurement is given by

$$\begin{aligned} \mathcal{L}_\gamma \hat{\rho} = & \hat{L}_\gamma \hat{\rho} \hat{L}_\gamma^\dagger - \frac{1}{2} \left( \hat{L}_\gamma^\dagger \hat{L}_\gamma \hat{\rho} + \hat{\rho} \hat{L}_\gamma^\dagger \hat{L}_\gamma \right) \\ & + (\hat{L}_\gamma \hat{\rho} + \hat{\rho} \hat{L}_\gamma^\dagger - \langle \hat{L}_\gamma + \hat{L}_\gamma^\dagger \rangle \hat{\rho}) \frac{dW}{dt} \end{aligned} \quad (3)$$

where the jump operator,  $\hat{L}_\gamma = \sqrt{\gamma} |C\rangle \langle C|$ , and  $dW$  is the Wiener increment associated with each measurement readout, being a zero mean random variable and obeying  $dW^2 = dt$  ( $dt$  being the time interval). Measurement strength is given by  $\gamma = \frac{e^4 V^2}{2\hbar^2 S_I} (T_0 - T_1)^2$  [24], where  $V$  is the voltage applied across the QPC,  $\hbar$  is Planck's constant,  $S_I$  is the shot noise associated with the QPC current, and  $T_0$  ( $T_1$ ) are the transmission probabilities of the QPC when the central dot is unoccupied (occupied).

We consider the situation where the reservoirs are at the same temperature, but have a large voltage bias across them, such that  $f(\varepsilon_L - \mu_L) \approx 1$  and  $f(\varepsilon_R - \mu_R) \approx 0$ . The local master equation is a valid approximation in this limit when  $\Omega \ll \Gamma_L, \Gamma_R$  [25]. Note that because of this large bias, our results here do not depend on  $\varepsilon$ . We use Eq. (2) to find a coupled differential equation for each element of  $\hat{\rho}$  (see Supplemental Material [26] for complete master equations), which are then solved numerically to arrive at the state evolution. Figures 2(a) and 2(b) respectively show the steady-state, ensemble-averaged result for the central dot occupation,  $\rho_{CC}$ , and the stochastic evolution of  $\rho_{CC}$  over time. In the

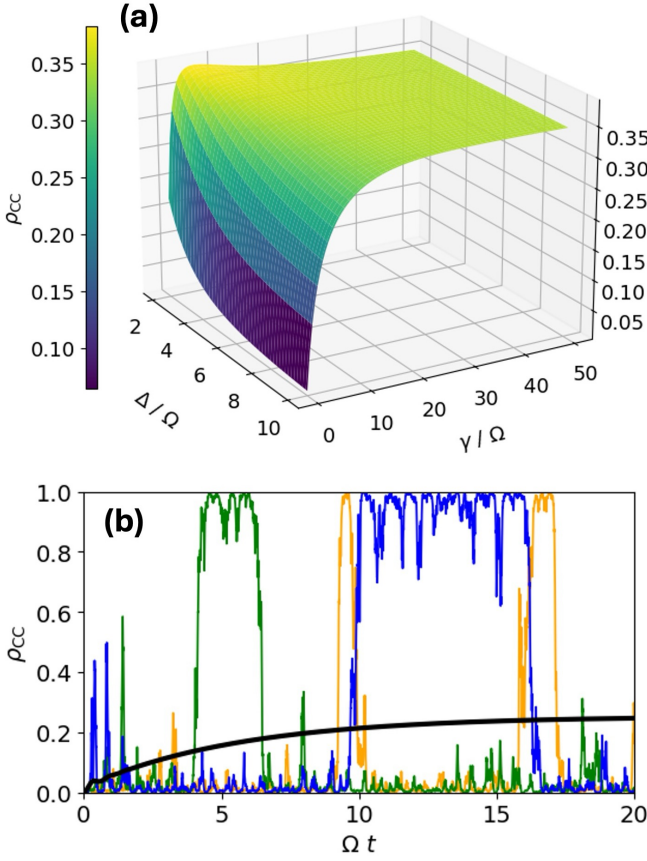


FIG. 2. (a) Steady state, ensemble averaged central dot occupation ( $\rho_{CC}$ ) for different values of  $\Delta$  and  $\gamma$ . (b) Stochastic evolution of the central dot occupation plotted vs time. The black curve shows the ensemble average, while the colored curves show time-averaged measurement realizations. Time averaging is done over a rectangular window of  $0.1 \Omega^{-1}$ . Initial state is a pure state with  $\rho_{LL} = 1$ , and all the other elements taken as zero. Other parameter values:  $\Gamma_L = 10 \Omega$ ,  $\Gamma_R = 8 \Omega$ ,  $\Delta = 10 \Omega$ ,  $\gamma = 10 \Omega$ , and  $dt = 10^{-4} \Omega^{-1}$ .

tunneling regime, when  $\Omega \ll \Delta$ ,  $\rho_{CC}$  is almost zero without measurement. While undergoing continuous monitoring, it quickly rises up to about  $1/3$ , and then saturates, with increasing measurement strength. Note that while the ensemble average value of  $\rho_{CC}$  saturates to a finite value smaller than 1, individual trajectories can occasionally reach unit probability. This strong dependence of  $\rho_{CC}$  on measurement suggests that the virtual state is indeed populated during tunneling. If it were not so, there would be no interaction between the electrons in the TQD and the QPC, and  $\rho_{CC}$  wouldn't be affected. Interestingly, the current through the TQD ( $I_T = \Gamma_R \rho_{RR}$ , in this regime) approaches zero with increasing  $\gamma$  [26].

Current through the QPC ( $I_Q$ ) for diffusive measurements is given by  $I_Q = \frac{e^2 V}{h} [T_0 + (T_1 - T_0)(\rho_{CC} + \frac{1}{\sqrt{\gamma}} \frac{dW}{dt})]$ . In Fig. 3, we study the correlations between these two currents. Fig. 3(a) shows the zero frequency cross-correlation [27] be-

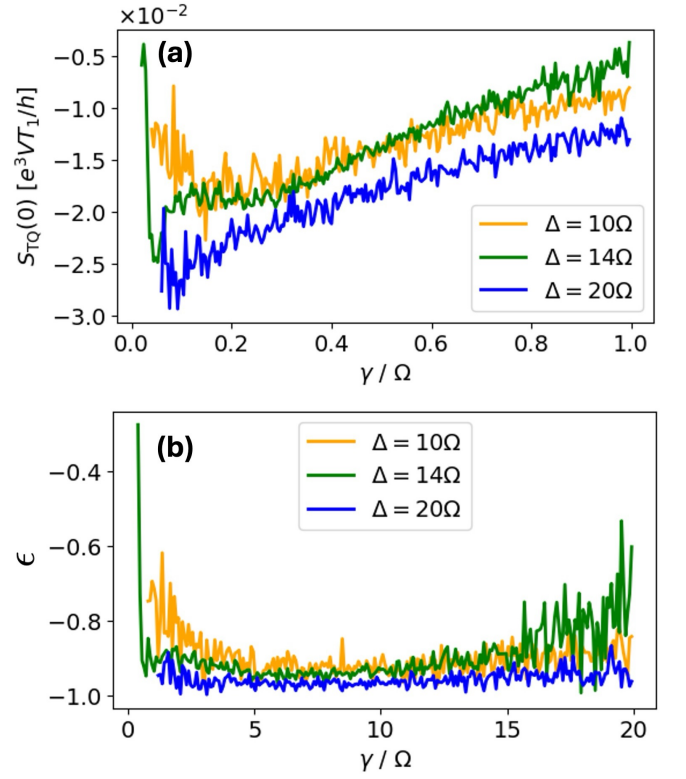


FIG. 3. Zero frequency cross correlation (a), and Pearson coefficient (b) between the current through the TQD and the detector as a function of measurement strength  $\gamma$ , for  $\Delta = 10 \Omega$ ,  $14 \Omega$  and  $20 \Omega$ ,  $\Gamma_L = 20 \Omega$  and  $\Gamma_R = 16 \Omega$ . Some low  $\gamma$  points in the plots for  $\Delta = 10 \Omega$ ,  $20 \Omega$  are omitted because of high noise.

tween  $I_T$  and  $I_Q$ , defined as

$$S_{TQ}(0) = \int_0^\infty dt \langle \delta I_T(t_0) \delta I_Q(t_0 + t) + \delta I_Q(t_0) \delta I_T(t_0 + t) \rangle, \quad (4)$$

where  $t_0$  is large enough such that the evolution has become stationary (no transient dynamics as in Fig. 2(b) black curve). We find that the currents are negatively correlated if  $T_0$  is lower than  $T_1$ . The Pearson coefficient, given by

$$\epsilon = \frac{S_{TQ}(0)}{\sqrt{S_{TT}(0)S_{QQ}(0)}} \quad (5)$$

and plotted in Fig. 3(b), gives the relative strength of cross-correlations between  $I_T$  and  $I_Q$  with respect to the auto-correlations of those currents. The auto-correlation terms are given by  $S_{ii}(0) = 2 \int_0^\infty dt \langle \delta I_i(t_0) \delta I_i(t_0 + t) \rangle$ , where  $i \in \{T, Q\}$ . We expect the cross correlations to approach zero as  $\gamma \rightarrow 0$ , which is what we get for  $\Delta = 14 \Omega$  in Fig. 3 (a). For  $\Delta = 10 \Omega$ ,  $20 \Omega$ , the numerical results for low  $\gamma$  (low enough to exhibit this behavior) get too noisy to be reliably included in the plot. As  $\gamma$  increases, the cross correlations do again approach zero for all shown values of  $\Delta$  as expected, since  $I_T$  itself approaches zero in this limit. Pearson coefficient also

shows similar behavior in Fig. 3 (b), but more importantly, the two currents are almost maximally anti-correlated ( $\epsilon \approx -1$ ) for a significant range of  $\gamma$ . Since both  $I_T$  and  $I_Q$  are experimentally accessible, comparing our theoretical predictions for  $S_{TQ}(0)$  with measured values provides a direct and effective means to validate our analysis.

*Quantum jump measurement*—We now consider a different limit of continuous measurement, where the transmittance of the QPC is much smaller than 1 and the electrons pass through its constriction via tunneling. We further assume that the transmittance is much bigger when C is not occupied compared to when it is (because of Coulomb repulsion), i.e.,  $T_0 \gg T_1$ . This implies that whenever an electron passes through the QPC, the occupation of the central dot jumps to zero [24]. In between these jumps, the system evolves smoothly. The stochastic master equation is now given by [24]

$$\hat{\rho}(t+dt) = dN(t) \frac{\hat{L}_\gamma \hat{\rho}(t) \hat{L}_\gamma^\dagger}{\text{Tr}[\hat{L}_\gamma \hat{\rho}(t) \hat{L}_\gamma^\dagger]} + (1 - dN(t)) \hat{\rho}^{\text{nj}}(t+dt), \quad (6)$$

where “nj” stands for no-jump,  $\hat{L}_\gamma = \sqrt{\gamma}(\mathbb{1} - |C\rangle\langle C|)$ , and  $dN(t)$  denotes the change in number of electrons detected at the QPC, which follows a binomial distribution of values 1 and 0 with probability  $\gamma(1 - \rho_{CC})dt$  and  $1 - \gamma(1 - \rho_{CC})dt$ , respectively. In between jumps, the evolution is given by

$$\begin{aligned} \hat{\rho}^{\text{nj}}(t+dt) = & \hat{\rho}(t) - \frac{i}{\hbar} [\hat{H}_{\text{TQD}}, \hat{\rho}] dt \\ & + (\mathcal{L}_{\Gamma_{L+}} \hat{\rho} + \mathcal{L}_{\Gamma_{R-}} \hat{\rho} + \mathcal{L}_\gamma \hat{\rho}) dt, \end{aligned} \quad (7)$$

where  $\mathcal{L}_{\Gamma_{L+}} \hat{\rho}$  and  $\mathcal{L}_{\Gamma_{R-}} \hat{\rho}$  have the same form as in the diffusive case, but  $\mathcal{L}_\gamma \hat{\rho} = \gamma[\frac{1}{2}(\hat{\rho}|C\rangle\langle C| + |C\rangle\langle C|\hat{\rho}) - \rho_{CC}\hat{\rho}]$ . Using these evolution equations, the result for the central dot occupation as a function of time is shown in Fig. 4 (a), along with the total number of electrons collected at the detector as a function of time,  $N(t) = \sum_{t_i=0}^t dN(t_i)$  (see the solid cyan curve). Although the detection of an electron in the QPC projects  $\rho_{CC}$  to zero, the no jump evolution leads to a relatively higher occupation, on average, compared with the no measurement scenario. This is to be expected since the ensemble average dynamics of jump measurement should be the same as that of diffusive measurement. We calculated an approximate analytic expression, in-between jumps, for  $\rho_{CC}$  in Fig. 4 (a) given by

$$\rho_{CC}(\tilde{t}) = \frac{2\Omega^2}{\Delta^2} e^{\tilde{t}/2} (1 - \cos(\tilde{t}\Delta)), \quad (8)$$

where  $\tilde{t}$  denotes the time since the last jump occurred. This expression, derived in the Supplemental Material [26], only holds when  $\Omega, \gamma \ll \Delta$  and for short periods of time after the jump. Frequent jumps due to measurements ensure that there is an excellent match between this and the numerical result. In Fig. 4 (b), we look at the same setup but with a higher measurement strength, which helps us sporadically catch the electron in C, with certainty, for significant intervals of time. This

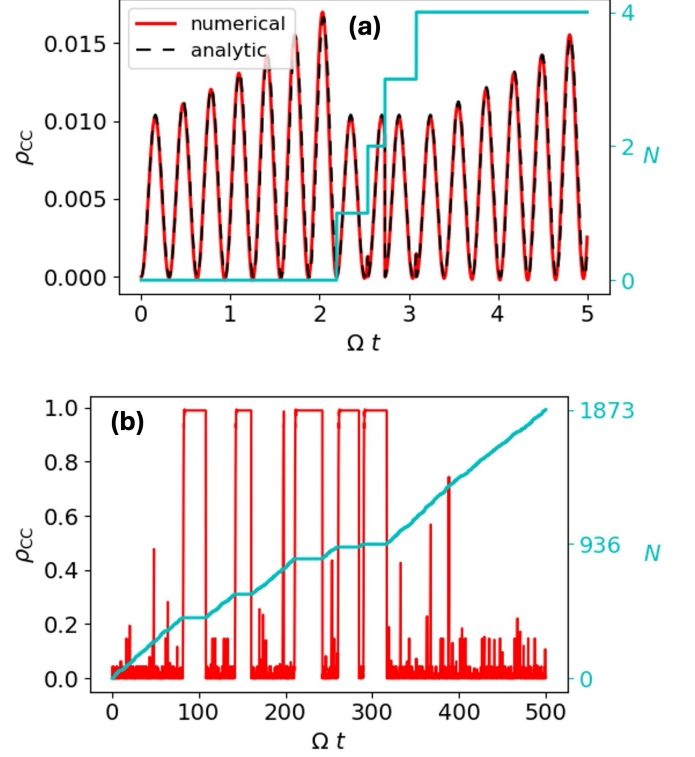


FIG. 4. (a,b) Central dot occupation ( $\rho_{CC}$ ) (left axis) and number of electrons (cyan, right axis) collected at the QPC detector ( $N$ ) as a function of time. Figure (a) contains both the numerical (red, solid) as well as an approximate analytic result (black, dashed).  $\gamma$  is taken to be  $0.5\Omega$  in (a) and  $5\Omega$  in (b). Rest of the parameters are common:  $\Delta = 20\Omega$ ,  $\Gamma_L = 20\Omega$ ,  $\Gamma_R = 16\Omega$ , and  $dt = 10^{-4}\Omega^{-1}$ . Initial state is taken to be the pure state  $|L\rangle\langle L|$ .

is analogous to stochastic diffusive trajectories often reaching unit occupation probability in C.

*Conclusions*—In this Letter, we investigate the interplay between virtual transitions and measurement back-action, proposing an experiment based on a triple quantum dot system under the continuous measurement of a highly-detuned central dot. We investigated the time evolution of the central dot occupation in both the diffusive and the jump quantum continuous measurement limits. Diffusive measurements result in noisy trajectories, while jump measurements result in smooth trajectories between jumps. In both measurement limits, however, the probability of average occupation of the central dot increases significantly due to measurement back-action, and saturates at a value of 1/3 as the measurement strength grows. Despite this saturation, as shown in Fig. S1 of the supplemental material, the current through the TQD setup,  $I_T \propto \rho_{RR}$ , asymptotically approaches zero with increasing measurement strength—demonstrating the quantum Zeno effect. We show that measurements can fundamentally alter the presence of an electron in the virtual state, offering a deeper insight into the role of observation in understanding the virtual states. Our results also indicate that in order to facilitate a current flow, the classically-forbidden central dot does indeed get



populated. The apparent paradox of observing the particle in the central dot, whether under weak or strong measurement, can be addressed by recognizing that the measurement process itself plays an active role in localizing the particle in the classically forbidden virtual state. The measurement process not only extracts information but also injects energy into the system, effectively enabling the particle to transiently occupy the virtual state. Notably, this suggests that quantum measurements could act as a thermodynamic resource, capable of powering transport processes that would otherwise be forbidden. Such a mechanism hints at novel strategies for designing measurement-driven quantum engines [28–40], where information gain and energy transfer are intrinsically intertwined, which we will explore further in Ref. [41].

*Acknowledgements*—ANS, BB, and ANJ acknowledge support from the John Templeton Foundation Grant ID 63209. RS acknowledges funding from the Spanish Ministerio de Ciencia e Innovación via grant No. PID2022-142911NB-I00, and through the “María de Maeztu” Programme for Units of Excellence in R&D CEX2023-001316-M.

- 
- [1] M. Büttiker and R. Landauer, Traversal Time for Tunneling, *Phys. Rev. Lett.* **49**, 1739 (1982).
- [2] R. Landauer and T. Martin, Barrier interaction time in tunneling, *Rev. Mod. Phys.* **66**, 217 (1994).
- [3] A. M. Steinberg, How much time does a tunneling particle spend in the barrier region?, *Phys. Rev. Lett.* **74**, 2405 (1995).
- [4] D. Shafir, H. Soifer, B. D. Bruner, M. Dagan, Y. Mairesse, S. Patchkovskii, M. Yu. Ivanov, O. Smirnova, and N. Dudovich, Resolving the time when an electron exits a tunnelling barrier, *Nature* **485**, 343 (2012).
- [5] Y. Choi and A. N. Jordan, Operational approach to indirectly measuring the tunneling time, *Phys. Rev. A* **88**, 052128 (2013).
- [6] R. Ramos, D. Spierings, I. Racicot, and A. M. Steinberg, Measurement of the time spent by a tunnelling atom within the barrier region, *Nature* **583**, 529 (2020).
- [7] J. Sinclair, D. Angulo, K. Thompson, K. Bonsma-Fisher, A. Brodutch, and A. M. Steinberg, Measuring the time atoms spend in the excited state due to a photon they do not absorb, *PRX Quantum* **3**, 010314 (2022).
- [8] K. Thompson, K. Li, D. Angulo, V.-M. Nixon, J. Sinclair, A. V. Sivakumar, H. M. Wiseman, and A. M. Steinberg, How much time does a photon spend as an atomic excitation before being transmitted?, *arXiv preprint arXiv:2310.00432* (2023).
- [9] A. Romito and Y. Gefen, Weak measurement of cotunneling time, *Phys. Rev. B* **90**, 085417 (2014).
- [10] O. Zilberberg, A. Carmi, and A. Romito, Measuring cotunneling in its wake, *Phys. Rev. B* **90**, 205413 (2014).
- [11] S. De Franceschi, S. Sasaki, J. M. Elzerman, W. G. van der Wiel, S. Tarucha, and L. P. Kouwenhoven, Electron Cotunneling in a Semiconductor Quantum Dot, *Phys. Rev. Lett.* **86**, 878 (2001).
- [12] K. Yamada, M. Stopa, T. Hatano, T. Ota, T. Yamaguchi, and S. Tarucha, Variation of co-tunneling and Kondo effects by control of the strength of coupling between a vertical dot and a two-dimensional electron gas, *Superlattices Microstruct.* **34**, 185 (2003).
- [13] R. Schleser, T. Ihn, E. Ruh, K. Ensslin, M. Tews, D. Pfannkuche, D. C. Driscoll, and A. C. Gossard, Cotunneling-Mediated Transport through Excited States in the Coulomb-Blockade Regime, *Phys. Rev. Lett.* **94**, 206805 (2005).
- [14] S. Gustavsson, M. Studer, R. Leturcq, T. Ihn, K. Ensslin, D. C. Driscoll, and A. C. Gossard, Detecting single-electron tunneling involving virtual processes in real time, *Phys. Rev. B* **78**, 155309 (2008).
- [15] O. Zilberberg and A. Romito, Sensing electrons during an adiabatic coherent transport passage, *Phys. Rev. B* **99**, 165422 (2019).
- [16] S. Amaha, T. Hatano, H. Tamura, S. Teraoka, T. Kubo, Y. Tokura, D. G. Austing, and S. Tarucha, Resonance-hybrid states in a triple quantum dot, *Phys. Rev. B* **85**, 081301 (2012).
- [17] M. Busl, G. Granger, L. Gaudreau, R. Sánchez, A. Kam, M. Pioro-Ladrière, S. A. Studenikin, P. Zawadzki, Z. R. Wasilewski, A. S. Sachrajda, and G. Platero, Bipolar spin blockade and coherent state superpositions in a triple quantum dot, *Nat. Nanotechnol.* **8**, 261 (2013).
- [18] F. R. Braakman, P. Barthelemy, C. Reichl, W. Wegscheider, and L. M. K. Vandersypen, Long-distance coherent coupling in a quantum dot array, *Nat. Nanotechnol.* **8**, 432 (2013).
- [19] R. Sánchez, G. Granger, L. Gaudreau, A. Kam, M. Pioro-Ladrière, S. A. Studenikin, P. Zawadzki, A. S. Sachrajda, and G. Platero, Long-range spin transfer in triple quantum dots, *Phys. Rev. Lett.* **112**, 176803 (2014).
- [20] S. Gustavsson, R. Leturcq, B. Simovič, R. Schleser, T. Ihn, P. Studerus, K. Ensslin, D. C. Driscoll, and A. C. Gossard, Counting statistics of single electron transport in a quantum dot, *Phys. Rev. Lett.* **96**, 076605 (2006).
- [21] T. Fujisawa, T. Hayashi, R. Tomita, and Y. Hirayama, Bidirectional Counting of Single Electrons, *Science* **312**, 1634 (2006).
- [22] M. A. Ratner, Bridge-assisted electron transfer: effective electronic coupling, *J. Phys. Chem.* **94**, 4877 (1990).
- [23] R. Sánchez, F. Gallego-Marcos, and G. Platero, Superexchange blockade in triple quantum dots, *Phys. Rev. B* **89**, 161402 (2014).
- [24] A. N. Jordan and I. A. Siddiqi, *Quantum Measurement* (Cambridge University Press, Cambridge, England, UK, 2024).
- [25] P. P. Potts, A. A. S. Kalaei, and A. Wacker, A thermodynamically consistent markovian master equation beyond the secular approximation, *New Journal of Physics* **23**, 123013 (2021).
- [26] See supplemental material for further information.
- [27] A. A. Clerk, M. H. Devoret, S. M. Girvin, F. Marquardt, and R. J. Schoelkopf, Introduction to quantum noise, measurement, and amplification, *Rev. Mod. Phys.* **82**, 1155 (2010).
- [28] C. Elouard and A. N. Jordan, Efficient quantum measurement engines, *Phys. Rev. Lett.* **120**, 260601 (2018).
- [29] C. Elouard, M. Waegell, B. Huard, and A. N. Jordan, An interaction-free quantum measurement-driven engine, *Foundations of Physics* **50**, 1294 (2020).
- [30] L. Bresque, P. A. Camati, S. Rogers, K. Murch, A. N. Jordan, and A. Auffèves, Two-Qubit Engine Fueled by Entanglement and Local Measurements, *Phys. Rev. Lett.* **126**, 120605 (2021).
- [31] J. Ferreira, T. Jin, J. Mannhart, T. Giamarchi, and M. Filippone, Transport and nonreciprocity in monitored quantum devices: An exact study, *Phys. Rev. Lett.* **132**, 136301 (2024).
- [32] B. Bhandari and A. N. Jordan, Continuous measurement boosted adiabatic quantum thermal machines, *Phys. Rev. Res.* **4**, 033103 (2022).
- [33] B. Bhandari, R. Czupryniak, P. A. Erdman, and A. N. Jordan, Measurement-Based Quantum Thermal Machines with Feedback Control, *Entropy* **25**, 204 (2023).
- [34] A. N. Jordan, C. Elouard, and A. Auffèves, Quantum measurement engines and their relevance for quantum interpretations,

- [Quantum Studies: Mathematics and Foundations](#) **7**, 203 (2020).
- [35] S. Gherardini, F. Campaioli, F. Caruso, and F. C. Binder, Stabilizing open quantum batteries by sequential measurements, [Phys. Rev. Res.](#) **2**, 013095 (2020).
- [36] M. T. Mitchison, J. Goold, and J. Prior, Charging a quantum battery with linear feedback control, [Quantum](#) **5**, 500 (2021), [2012.00350v2](#).
- [37] T. Zhang, H. Yang, and S.-M. Fei, Local-projective-measurement-enhanced quantum battery capacity, [Phys. Rev. A](#) **109**, 042424 (2024).
- [38] M. H. Mohammady and J. Anders, A quantum Szilard engine without heat from a thermal reservoir, [New J. Phys.](#) **19**, 113026 (2017).
- [39] K. Yanik, B. Bhandari, S. K. Manikandan, and A. N. Jordan, Thermodynamics of quantum measurement and maxwell's demon's arrow of time, [Phys. Rev. A](#) **106**, 042221 (2022).
- [40] P. A. Erdman, R. Czupryniak, B. Bhandari, A. N. Jordan, F. Noé, J. Eisert, and G. Guarnieri, Artificially intelligent maxwell's demon for optimal control of open quantum systems, [arXiv:2408.15328](#) (2024).
- [41] R. Sánchez *et al.*, manuscript under preparation.

# Supplemental Material for “Capturing an electron in the virtual state”

Alok Nath Singh,<sup>1,2</sup> Bibek Bhandari,<sup>2</sup> Rafael Sánchez,<sup>3,4,5</sup> and  
Andrew N. Jordan<sup>2,1,6</sup>

<sup>1</sup>Department of Physics and Astronomy, University of Rochester, Rochester, NY 14627, USA

<sup>2</sup>Institute for Quantum Studies, Chapman University, Orange, CA 92866, USA

<sup>3</sup>Departamento de Física Teórica de la Materia Condensada, Universidad Autónoma de Madrid, 28049 Madrid, Spain

<sup>4</sup>Condensed Matter Physics Center (IFIMAC), Universidad Autónoma de Madrid, 28049 Madrid, Spain

<sup>5</sup>Instituto Nicolás Cabrera (INC), Universidad Autónoma de Madrid, 28049 Madrid, Spain

<sup>6</sup>The Kennedy Chair in Physics, Chapman University, Orange, CA 92866, USA

## S-I. STOCHASTIC MASTER EQUATION

We discuss here the stochastic master equation (SME) for the diffusive continuous measurement limit, along with the individual differential equations obtained for each density matrix element. The SME for the infinite bias case is given by

$$\frac{d\hat{\rho}}{dt} = -\frac{i}{\hbar}[\hat{H}_{\text{TQD}}, \hat{\rho}] + \mathcal{L}_{\gamma, L+}\hat{\rho} + \mathcal{L}_{\gamma, R-}\hat{\rho} + \mathcal{L}_{\gamma}\hat{\rho}, \quad (\text{S1})$$

with the Lindblad superoperators associated with the reservoirs

$$\mathcal{L}_{\gamma, L+}\hat{\rho} = \Gamma_L \left[ \rho_{00}\hat{\Pi}_{LL} - \frac{1}{2}(\hat{\Pi}_{00}\hat{\rho} + \hat{\rho}\hat{\Pi}_{00}) \right], \quad (\text{S2})$$

$$\mathcal{L}_{\gamma, R-}\hat{\rho} = \Gamma_R \left[ \rho_{RR}\hat{\Pi}_{00} - \frac{1}{2}(\hat{\Pi}_{RR}\hat{\rho} + \hat{\rho}\hat{\Pi}_{RR}) \right], \quad (\text{S3})$$

and with the measurement

$$\mathcal{L}_{\gamma}\hat{\rho} = \gamma \left[ \rho_{CC}\hat{\Pi}_{CC} - \frac{1}{2}(\hat{\Pi}_{CC}\hat{\rho} + \hat{\rho}\hat{\Pi}_{CC}) + (\hat{\Pi}_{CC}\hat{\rho} + \hat{\rho}\hat{\Pi}_{CC} - 2\rho_{CC}\hat{\rho})\frac{dW}{dt} \right], \quad (\text{S4})$$

where  $\rho_{mn}$  stands for  $\langle m|\rho|n\rangle$ , and  $\hat{\Pi}_{mn}$  stands for the projector operator  $|m\rangle\langle n|$  with  $m, n \in \{L, C, R\}$ .  $dW$  is the Gaussian noise associated with each measurement readout, having a zero mean and a standard deviation equal to  $\sqrt{dt}$  ( $dt$  being the time interval between measurements).

Breaking down Eq. (S1) into differential equations for individual density matrix elements, we get

$$\dot{\rho}_{LL} = -i\Omega(\rho_{CL} - \rho_{LC}) + \Gamma_L\rho_{00} - 2\sqrt{\gamma}\rho_{CC}\rho_{LL}\frac{dW}{dt}, \quad (\text{S5})$$

$$\dot{\rho}_{RR} = -i\Omega(\rho_{CR} - \rho_{RC}) - \Gamma_R\rho_{RR} - 2\sqrt{\gamma}\rho_{CC}\rho_{RR}\frac{dW}{dt}, \quad (\text{S6})$$

$$\dot{\rho}_{CC} = -i\Omega(\rho_{LC} - \rho_{CL} + \rho_{RC} - \rho_{CR}) + 2\sqrt{\gamma}\rho_{CC}(1 - \rho_{CC})\frac{dW}{dt}, \quad (\text{S7})$$

$$\dot{\rho}_{LC} = -i(\Omega\rho_{CC} - \Delta\rho_{LC} - \Omega\rho_{LL} - \Omega\rho_{LR}) - \frac{\gamma}{2}\rho_{LC} - 2\sqrt{\gamma}\rho_{LC}(\rho_{CC} - \frac{1}{2})\frac{dW}{dt}, \quad (\text{S8})$$

$$\dot{\rho}_{RC} = -i(\Omega\rho_{CC} - \Delta\rho_{RC} - \Omega\rho_{RR} - \Omega\rho_{RL}) - \frac{\Gamma_R + \gamma}{2}\rho_{RC} - 2\sqrt{\gamma}\rho_{RC}(\rho_{CC} - \frac{1}{2})\frac{dW}{dt}, \quad (\text{S9})$$

$$\dot{\rho}_{LR} = -i\Omega(\rho_{CR} - \rho_{LC}) - \frac{\Gamma_R}{2}\rho_{LR} - 2\sqrt{\gamma}\rho_{CC}\rho_{LR}\frac{dW}{dt}. \quad (\text{S10})$$

To obtain the results shown for the diffusive limit in the article, we solve the above equations numerically. The ensemble average evolution can be obtained by dropping the stochastic terms in these equations.

## S-II. TRIPLE QUANTUM DOT CURRENT

In Fig. 2(a) of the main text we plot the steady state, ensemble averaged  $\rho_{CC}$  as a function of  $\Delta$  and  $\gamma$ . In Fig. S1 we complement this result by plotting the steady state, ensemble averaged current through the TQD ( $I_T$ ) as a function of  $\Delta$  and  $\gamma$  in the same configuration. The current approaches zero for large tunnel barrier ( $\Delta$ ) and no measurement ( $\gamma = 0$ ). Moreover, for any value of  $\Delta$ , current also approaches zero

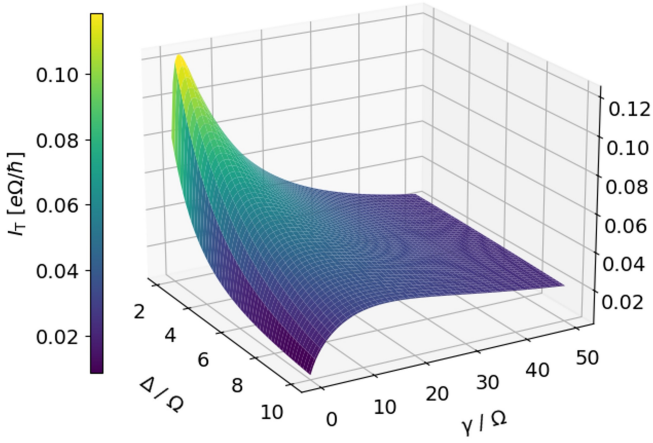


FIG. S1. Steady state, ensemble averaged TQD current ( $I_T$ ) for different values of  $\Delta$  and  $\gamma$ .

for strong measurements (large  $\gamma$ ). In this regime, we observe the quantum Zeno effect, where continuous monitoring traps the electron in the central dot for extended periods of time.

### S-III. QUANTUM JUMP CASE: ANALYTIC EXPRESSION

The state evolution for the quantum jump limit of measurement looks simple enough to warrant an analytic expression,

when  $\gamma \ll \Delta$ , as shown in Fig. 4 of the main text. It follows the structure of a sinusoidal oscillation increasing in amplitude with time. Frequent jumps ensure that  $\rho_{CC}$  and  $\rho_{RR}$  remains close to zero, while  $\rho_{LL}$  is close to one. To derive the analytic expression, we thus assume  $\rho_{RR} = 0$ ,  $\rho_{LL} = 1$ , and  $\rho_{CC} \ll \rho_{LL}$ . The coherence between the left and the right dot,  $\rho_{LR}$ , is also negligible since  $\Omega \ll \Delta$ , and thus, it is taken to be 0. All of these assumptions were verified by the numerics to have a negligible effect on the evolution. The differential equations left to solve are

$$\dot{\rho}_{CC} = 2\Omega \text{Im} \rho_{LC} + \gamma \rho_{CC}, \quad (\text{S11})$$

$$\text{Re} \dot{\rho}_{LC} = -\Delta \text{Im} \rho_{LC} + \gamma \text{Re} \rho_{LC}/2, \quad (\text{S12})$$

$$\text{Im} \dot{\rho}_{LC} = \Omega + \Delta \text{Re} \rho_{LC} + \gamma \text{Im} \rho_{LC}/2. \quad (\text{S13})$$

By substitution, this reduces to a single third order differential equation, which can be exactly solved. The analytic expression for  $\rho_{CC}$ , in between jumps, is then given by

$$\rho_{CC}(t) = 2 \frac{\Omega^2}{\Delta^2} e^{\gamma t/2} (1 - \cos t\Delta), \quad (\text{S14})$$

under these approximations.